Electron-spin-resonance study of the one-dimensional magnet (NH4)2MnF5

Alexander Krimmel, Hans-Albrecht Krug von Nidda, Alois Loidl, Hans Moritz Mangold, J. Pebler

Angaben zur Veröffentlichung / Publication details:

Krimmel, Alexander, Hans-Albrecht Krug von Nidda, Alois Loidl, Hans Moritz Mangold, and J. Pebler. 2002. "Electron-spin-resonance study of the one-dimensional magnet (NH4)2MnF5." *Journal of Physics: Condensed Matter* 14 (17): 4585–94. https://doi.org/10.1088/0953-8984/14/17/328.

Electron-spin-resonance study of the one-dimensional magnet $(NH_4)_2MnF_5$

A Krimmel[1], H-A Krug von Nidda[1], A Loidl[1], M Mangold[2] and J Pebler[2]

[1] Experimentalphysik V, Elektronische Korrelationen und Magnetismus, Institut für Physik, Universität Augsburg, D-86159 Augsburg, Germany
[2] Fachbereich Chemie, Philipps Universität, D-35043 Marburg, Germany

Abstract

Electron-spin-resonance (ESR) experiments have been performed on the quasi-one-dimensional magnet $(NH_4)_2MnF_5$. The ESR spectrum consists of two components, an extremely broad signal and a weak but sharp resonance on top of the broad signal. The resonance field of the dominating broad signal is most probably shifted by strong non-diagonal terms of the dynamic susceptibility to g-values well below $g = 2$ and becomes undetectable upon the onset of strong one-dimensional correlations below $T \leqslant 60$ K. We attribute these two signals to Mn^{3+} ions of the chains (broad resonance, intrinsic response of the sample) and to defects (small resonance), respectively. The ESR spectra reflect the evolution from the paramagnetic state ($T > 60$ K) to one-dimensional magnetic behaviour ($T \leqslant 60$ K). The results are discussed with respect to the local anisotropy of the Mn^{3+} ions and comparison is made with the behaviour of other one-dimensional magnetic compounds.

1. Introduction

One-dimensional magnetic systems have attracted considerable interest in solid-state physics. For topological reasons, short-range-order effects of interacting spins and non-linear excitations are essential in describing the spin dynamics of these compounds [1]. The physical realizations of one-dimensional magnets are compounds in which the magnetic ions are arranged along chains. Consequently, the exchange interaction J along the chains is significantly stronger than the exchange constant J' perpendicular to it. The ratio J'/J can be taken as a measure of the one dimensionality of a system. The existence of a non-vanishing inter-chain coupling J' necessarily leads to a three-dimensional long-range magnetically ordered state at sufficiently low temperatures. However, the typical features of one-dimensional magnetic behaviour can be observed over a large temperature range above the ordering temperature. The fluoromanganites are antiferromagnetic chain compounds which may serve as model systems for one-dimensional magnets [2]. Previously, the spin dynamics of

$A^{I}_{2}/A^{II}MnF_5(H_2O)$ (with A = Li^+, Na^+, NH^+_4, ND^+_4, K^+, Sr^{2+}, Ba^{2+} and enH^{2+}_2 (en = ethylene diamine)) was studied for ^{57}Fe-doped compounds by means of Mössbauer spectroscopy [2–7]. The relaxation spectra were calculated and interpreted on the basis of classical soliton theory for $T_N \leqslant T \leqslant 3T_N$. In particular, the magnetic properties of $(ND_4)_2MnF_5$ have recently been investigated in detail by means of neutron scattering experiments [8]. The deuterated sample has been chosen in order to avoid strong incoherent background scattering of hydrogen. From a crystallographic point of view, deuterated and protonated compounds are equivalent. From the spin-wave dispersion, the exchange and anisotropy parameters of the Mn^{3+} spins which form the chains were deduced as $J/k_B = -10.3(1)$ K and $D/k_B = -2.78(2)$ K, in excellent agreement with the results of susceptibility measurements [8]. The measurements of the non-linear excitations resulted in a soliton activation energy of $E_S/k_B = 81(3)$ K [8]. The temperature dependence of the inverse magnetic correlation length revealed an exponential increase typical for strongly anisotropic systems. However, the values of the anisotropy constant D and the exchange constant J are of the same order of magnitude. Therefore, the present compound is neither a Heisenberg (purely isotropic) nor an Ising (infinite anisotropy) system, but should be considered as being located between these two limiting cases. Here we report on a detailed ESR study of the one-dimensional magnet $(NH_4)_2MnF_5$ carried out in order to investigate the role of the local anisotropy.

2. Experimental details

Single-crystalline samples have been prepared by the evaporation method as described previously [8]. Characterization by x-ray and neutron diffraction showed perfect homogeneity and excellent quality of the samples. $(NH_4)_2MnF_5$ crystallizes in orthorhombic symmetry with space group $Pnma$ and four formula units per unit cell. The magnetic species Mn^{3+} is in its high-spin configuration with $S = 2$. The magnetic ions are octahedrally coordinated by fluorine ions. Due to a cooperative Jahn–Teller effect, the octahedra are significantly elongated and trans-corner-linked to form chains which are separated by the cations. An increase in size of the cations results in a widening of the (Mn–F–Mn) bridge angle β. For $(NH_4)_2MnF_5$ the ammonium ions cause a (Mn–F–Mn) bridge angle of 139.5°. Additional to the antiferromagnetic spin arrangement along the chains (crystallographic b-axis) below $T_N = 8.5$ K, a spin canting (with a canting angle of about 4°) resulting in a weak ferromagnetic component along the a-axis is observed. In the equatorial plane perpendicular to the chain axis, the Mn–F distances differ by <0.1% and therefore the coordination around the Mn(III) ions reveals an almost ideal axial symmetry (D_{4h}).

Electron-spin resonance (ESR) measures the absorption P_{abs} of the transverse magnetic microwave field with frequency ν as a function of a static externally applied magnetic field $\vec{B}$. The ESR experiments were performed using a Bruker ELEXSYS E500 spectrometer working at X-band frequencies (9.4 GHz) in continuous-wave (CW) mode (field sweeps at fixed microwave frequency). The external magnetic field $\vec{B}$ was applied horizontally and the magnetic component $\vec{h}$ of the linearly polarized microwave field was oriented vertically. Hence, the direction of the magnetic microwave field coincided with the rotation axis of the goniometer, which was used to measure the orientation dependence of the ESR spectra. To improve the signal-to-noise ratio, the derivative of the absorption dP_{abs}/dB was detected by the lock-in technique with field modulation. A He-gas continuous-flow cryostat (Oxford Instruments) was employed to allow measurements between 4 K and room temperature. Some additional EPR measurements were carried out at the High-Field Laboratory, Grenoble, at $T = 100$ K, for frequencies $\nu = 115$, 190, 230 and 285 GHz, respectively in fields up to 12 T.

3. Results and discussion

3.1. ESR spectra

We measured the angular dependence of the paramagnetic resonance in $(NH_4)_2MnF_5$ with respect to the static external magnetic field for the three crystallographic planes *a–b*, *b–c* and *a–c*, where the incident microwave field $\vec{h}$ was applied parallel to the vertical rotation axis corresponding to the crystallographic *c*-, *a*- and *b*-axis, respectively. The measurements were performed with an angular step width of 10° from 0° to 180°. Figure 1 shows ESR spectra at $T = 200$ K for each of the three rotation planes for which the crystal has been oriented with one of its crystallographic axis parallel to the horizontally applied field. One can distinguish two qualitatively different behaviours. A small resonance around a resonance field $B_{res} \approx 0.33$ T corresponding to $g \approx 2$ can be observed for all orientations. The halfwidth at half-maximum of this small resonance is about $\Delta B(\mathrm{HWHM}) \approx 0.026$ T. For $\vec{b} \parallel \vec{h}$, an additional broad resonance ($\Delta B \approx 0.65$ T) appears, which is centred around $B_{res} \approx 0.66$ T. This dominating signal is strongly suppressed for $\vec{a} \parallel \vec{h}$ and additionally shifted for $\vec{c} \parallel \vec{h}$. We thus observe a pronounced angular dependence with respect to the polarization direction of the microwave field.

Among the compounds which have been used in ESR studies on one-dimensional spin systems, $(NH_4)_2MnF_5$ shows striking similarities with $CsNiF_3$, the best known example of a ferromagnetic spin chain. Though $CsNiF_3$ is a ferromagnet, in contrast to $(NH_4)_2MnF_5$, it should be noted that the modulus of the exchange constants J and the crystal-field splitting parameters D are very similar. ESR measurements on $CsNiF_3$ were performed by Benner *et al* [9] in order to study the influence of non-diagonal elements of the dynamic susceptibility on the ESR signal. The ESR signal of Ni^{2+} in $CsNiF_3$ is characterized by an extremely broad resonance with a corresponding linewidth of $\Delta B \approx 0.75$ T centred around $B_{res} \approx 0.75$ T. In the present case of $(NH_4)_2MnF_5$, we also observe a broad resonance with a linewidth of the same order of magnitude. Again, the linewidth corresponds to the value of the resonance field. To give a rough estimate of the linewidth expected, we compare the zero-field-splitting energy D with the magnetic exchange interaction J. According to the theory of exchange narrowing [10], we obtain a value of $\Delta B \propto \langle \Delta E_{CF}^2 \rangle / E_{ex} \approx D^2/J$ of about $\approx$1 T for both compounds, in good agreement with the experimental observation. Furthermore, a small structure on top of the broad signal around $g \approx 2$ is found for both compounds and, in the case of $CsNiF_3$, has been attributed to defects in the chains or impurities [9].

The ESR spectra of $CsNiF_3$ show a comparable dependence on the polarization of the microwave field. Like for $(NH_4)_2MnF_5$, the strongest ESR signal is observed for the chain axis parallel to the direction of the magnetic microwave field and becomes strongly suppressed for the microwave field applied perpendicular to the chain direction. This effect is caused by the influence of the large non-diagonal terms $\chi^{+-}(\omega)$ and $\chi^{-+}(\omega)$ of the dynamic susceptibility [9]. Pronounced non-diagonal terms arise in addition to the usually observed circularly polarized components $\chi^{++}(\omega)$ and $\chi^{--}(\omega)$ if a spin system is governed by interactions of low symmetry and exhibits a sufficiently broad ESR line $\Delta B \approx B_{res}$. This is often the case in one-dimensional magnetic chain compounds, since the strong anisotropy of the spin systems provides for interactions of low symmetry and the dominating contribution of spin diffusion leads to a partial suppression of the exchange narrowing, which in turn results in broad ESR lines.

In the case of sufficient exchange narrowing, the spectra can be approximated by the following expression:

$$\frac{\mathrm{d}P_{abs}}{\mathrm{d}B} = A\frac{\mathrm{d}}{\mathrm{d}B}\left(\frac{\Delta B + \alpha(B - B_{res})}{(B - B_{res})^2 + \Delta B^2} + \frac{\Delta B + \alpha(B + B_{res})}{(B + B_{res})^2 + \Delta B^2}\right) + \mathrm{BG}. \qquad (1)$$

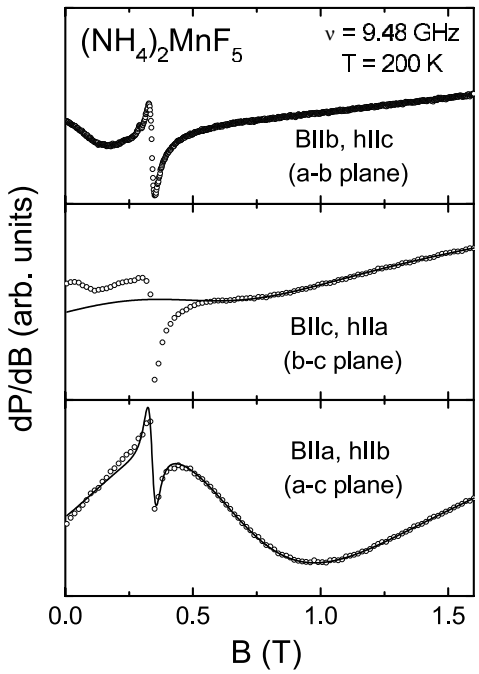

Figure 1. ESR spectra of $(NH_4)_2MnF_5$ at $T = 200$ K for one of the three crystallographic axes parallel to the microwave-polarization direction and another parallel to the horizontally applied field $\vec{B}$. The full curve corresponds to a fit of the measured intensities according to equation (1) (see the text). The parameters of the fit for $\vec{B} \parallel \vec{a}, \vec{h} \parallel \vec{b}$ (lower frame) are presented in detail in figure 2. For $\vec{B} \parallel \vec{c}, \vec{h} \parallel \vec{a}$ (middle frame) the fit has been performed with $\alpha = -0.5$ (see the text).

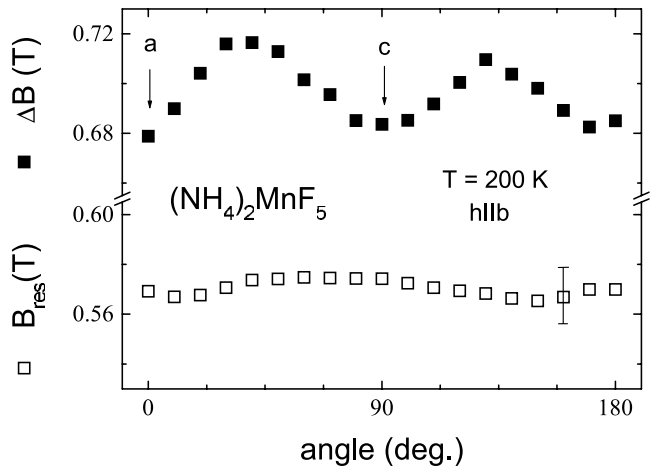

Figure 2. Angular dependences of the ESR linewidth (upper part) and resonance field (lower part) of the dominating broad resonance of $(NH_4)_2MnF_5$ at $T = 200$ K. A dispersion-to-absorption ratio of $\alpha = 0.37$ accounted best for the observed asymmetry. This parameter was fixed for the given microwave polarization direction $\vec{h} \parallel \vec{a}$.

Equation (1) corresponds to an asymmetric Lorentzian line of amplitude A, which includes both circular absorption contributions of the dynamic susceptibility at $\pm B_{\rm res}$, and the non-diagonal elements appear as some kind of dispersion, where α denotes the dispersion-to-absorption ratio. The background (BG) due to microphony from field modulation is assumed to be linearly dependent on the applied magnetic field. The spectrum for $\vec{h} \parallel \vec{b}$ in the lower frame of figure 1 is very well described by equation (1), adding an additional Lorentzian line for the small resonance on top of the broad line. Figure 2 shows the orientation dependence of the corresponding resonance field and linewidth at $T = 200$ K. Within the a–c plane, the orientation dependence is weak, with a mean resonance field of $\langle B_{res} \rangle = 0.57 \pm 0.02$ T, consistent with a weak anisotropy perpendicular to the chain direction (crystallographic b-axis). The angular dependence of the linewidth is also weak but exhibits approximately a 90° periodicity, as expected due to the crystal symmetry. To verify the influence of the non-diagonal elements $\chi^{+-}(\omega)$ and $\chi^{-+}(\omega)$ on changing microwave polarization, we simulated the spectra for $\vec{B} \parallel \vec{c}$ and $\vec{h} \parallel \vec{a}$ with the same resonance field and linewidth as for $\vec{B} \parallel \vec{c}$, $\vec{h} \parallel \vec{b}$, just changing the parameter α. The result is shown in the middle frame of figure 1. Despite some deviation at low field, the approximation of the experimental curve is quite satisfactory. We therefore conclude that the observed pronounced orientation dependence of the ESR spectra on the microwave-polarization direction can be attributed to the non-diagonal terms of the dynamic susceptibility which may be described phenomenologically by a dispersion-to-absorption ratio α.

However, we have to consider critically the difficulties of performing such an analysis. The description of the ESR spectra by a Lorentzian line is strictly valid only in the limit $D \ll J$. As mentioned above, the zero-field splitting and the exchange constant are of the same order of magnitude. At X-band frequencies, the microwave energy is significantly smaller than the crystal-field splitting and consequently the applied magnetic field is too small to fully cover all possible dipole transitions. The comparably weak exchange narrowing may be insufficient to concentrate the intensity into a single Lorentzian line. This becomes evident at lower temperatures. The temperature dependence of the ESR spectra obtained for $\vec{h} \parallel \vec{b}$ is shown in figure 3 together with the corresponding fits according to equation (1). For the given measurement geometry, α has been kept constant. Below $T \leqslant 100$ K the broad resonance splits into two lines that have been taken into account for the fit curves. One of them shifts to high fields and becomes unobservable below 50 K, whereas the other remains near zero field.

Here the additional spectra obtained from high-field ESR measurements at the High-Field Laboratory, Grenoble, can clarify the situation. The EPR spectra were recorded at $T = 100$ K for $\nu = 115$, 190, 230 and 285 GHz. The result for $\nu = 190$ GHz is shown in figure 4. We observe a single resonance line without any fine structure, which is well fitted by a single Lorentzian line without dispersive contributions, because the resonance field clearly exceeds the linewidth. The absence of a fine structure shows that the exchange narrowing is sufficiently strong to concentrate all spectral weight into a single resonance line. The linewidth $\Delta B \approx 1$ T is approximately as large as in case of the X-band ESR measurements. As can be obtained from the inset in figure 4, the resonance field is found to be close to the spin-only value $g = 2$, which is typical for 3d ions, where the orbital momentum is quenched. The strong deviation of the resonance field from $g = 2$, which is observed at X-band frequencies, is therefore fully explained by the influence of the crystal-field anisotropy and the interplay of the different components of the dynamic susceptibility.

The successful fitting of the spectra obtained at X-band frequencies for $\vec{h} \parallel \vec{b}$ and the sufficient exchange narrowing of the spectra observed at high frequencies justify an approximate treatment of the ESR data by means of equation (1) at least for temperatures above 100 K. At lower temperatures one can account for the splitting by introducing an

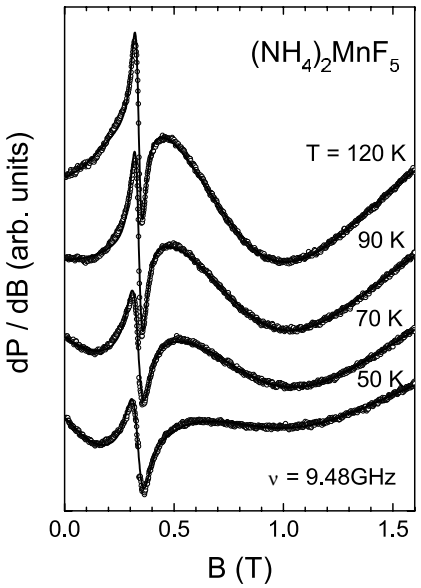

Figure 3. The temperature dependence of the ESR spectra of $(NH_4)_2MnF_5$ for measuring geometry $\vec{B} \parallel \vec{a}$ and $\vec{h} \parallel \vec{b}$. At $T = 120$ K, the full curve corresponds to a fit of a narrow and a broad resonance according to equation (1). At lower temperatures a good fit to the data could only be achieved by assuming an additional splitting of the broad resonance into two Lorentzian lines.

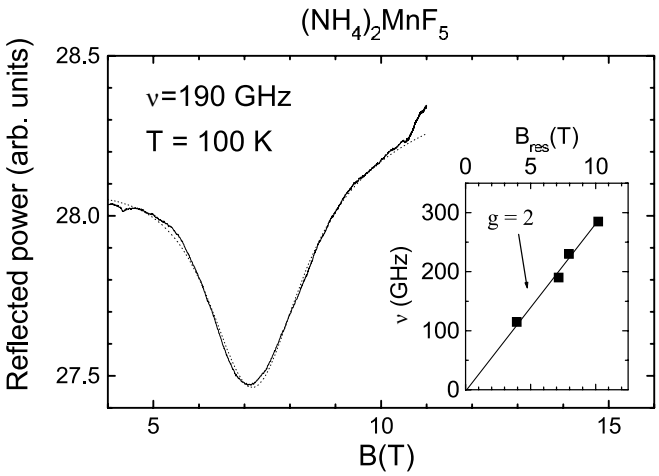

Figure 4. The ESR spectrum of $(NH_4)_2MnF_5$ at $T = 100$ K for frequency $\nu = 190$ GHz. The full curve refers to the measured intensity and the dotted curve indicates a Lorentzian fit to the data. The inset shows the resonance fields for different frequencies which are evidently consistent with a $g = 2$ resonance (straight line).

additional Lorentzian line, which is located near zero field and allows a reasonable description of the ESR spectra, as is shown in figure 3. In the following, we discuss the temperature dependence of the broad and narrow resonance separately.

3.2. Main resonance

At X-band frequencies, the dominating broad ESR signal of $(NH_4)_2MnF_5$ is observed for $\vec{h} \parallel \vec{b}$ and can be described by a single Lorentzian line at high temperatures $T \geqslant 100$ K. The temperature dependence of the linewidth, resonance field and absorbed intensity $I = A\,\Delta B^2(1+\alpha^2)^{1/2}$ of this resonance, as determined by means of equation (1), are shown in figure 5. Above 100 K the resonance field remains approximately constant near 0.6 T. The linewidth of $\Delta B \approx 0.65$ T at elevated temperatures ($200 \leqslant T \leqslant 300$ K) starts to increase upon decreasing temperature up to about 0.9 T at 100 K. In the same temperature regime, the intensity follows a Curie–Weiss law $I \propto (T-\Theta)^{-1}$, as is illustrated in the inset of figure 5, where we have plotted the inverse ESR intensity versus temperature. The corresponding Curie–Weiss temperature of $\Theta = -68$ K is in good agreement with the results of susceptibility measurements [11]. This agreement again justifies the evaluation of the spectra above 100 K using equation (1), as the ESR intensity should be proportional to the spin susceptibility of the sample. Below $T \leqslant 100$ K, the broad ESR signal starts to split into two lines (open symbols in figure 5). One line shifts to higher resonance fields upon decreasing temperature but, simultaneously, becomes suppressed (decreasing intensity, as shown in the lower frame of figure 5) and finally undetectable at low temperatures. The second resonance is located around $B_{res} \approx 0$. The fit of the broad resonance by two lines below $T \leqslant 100$ K not only results in a good description of the ESR spectra (compare also with figure 2) but also can be physically justified. As mentioned above, the ESR intensity should be proportional to the spin susceptibility. Assuming a splitting of the broad resonance into two lines yields to a temperature-dependent intensity (open squares in figure 5) similar to the temperature dependence of the magnetic susceptibility of $(NH_4)_2MnF_5$. The corresponding characteristic susceptibility maximum of one-dimensional magnetic systems is indicated by T_{max}, which has been determined by single-crystal magnetic susceptibility measurements on $(NH_4)_2MnF_5$ [11].

To obtain a more quantitative estimate of the intensity, we have additionally performed measurements on the reference compound Gd_2BaCuO_5 with a Curie–Weiss temperature $\Theta = -30$ K using the same spectrometer settings. The electronic configuration of Gd^{3+} ions is a pure spin state with $S = 7/2$ and $L = 0$. From the masses of the samples (6.78 mg for Gd_2BaCuO_5 and 8.13 mg for $(NH_4)_2MnF_5$, respectively) the number of spins contributing to the ESR signal is known. Then the intensity of the broad ESR signal of $(NH_4)_2MnF_5$ can be accounted for, assuming that the Mn^{3+} ions are in the high-spin state ($S = 2$) with $g = 2$ and a corresponding quenched orbital momentum ($L = 0$), as expected. These calibration measurements reveal that almost all of the Mn^{3+} ions contribute to this signal and therefore it is considered as the intrinsic response of the compound to the perturbation by an applied electromagnetic field. This is remarkable for the reason detailed below.

In $(NH_4)_2MnF_5$ the octahedral field of the fluorine ions splits the five d orbitals ($^5D_0$) of Mn^{3+} into a triplet t_{2g} and a doublet e_g with an energy splitting of the order of 10^4 K [4, 12]. In the case of intermediate ligand fields the dominating Hund's coupling causes a parallel spin alignment of the four d electrons, where three of them occupy the triplet t_{2g} state and the fourth is found in the e_g state, leading to a high-spin configuration ($S = 2$). Including the spin, the Γ_3 ground state is tenfold degenerate. This degeneracy is lifted by second-order spin–orbit coupling. In this case the Zeeman effect is very complicated and it is unlikely that one will observe an ESR signal at all [12]. However, the Jahn–Teller theorem is applicable for Mn^{3+} in octahedral symmetry. This changes the situation drastically. The Jahn–Teller effect reduces the octahedral ligand field to axial symmetry, reflected in remarkably lengthened MnF_6 octahedra. The orbital degeneracy of the e_g ground state is removed, resulting in two singlets

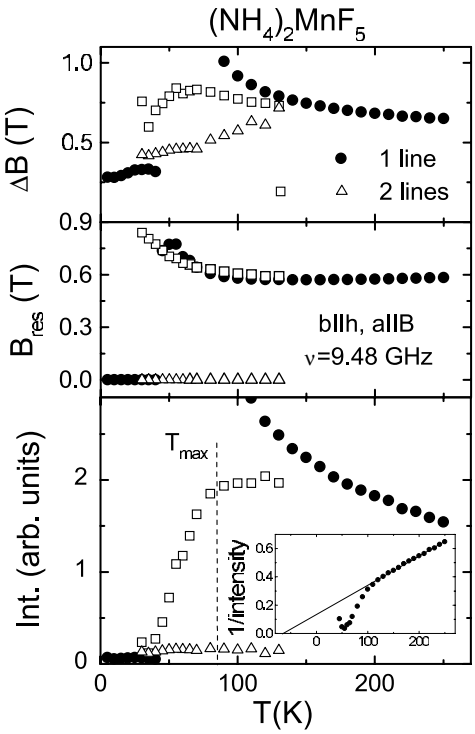

Figure 5. Temperature dependences of the main ESR resonance of $(NH_4)_2MnF_5$ for $\vec{a} \parallel \vec{B}$ and $\vec{b} \parallel \vec{h}$: linewidth (upper panel), resonance field (central part) and intensity (lower panel). Full circles and open symbols refer to a fit of the ESR spectra by a single Lorentzian line and a superposition of two different lines, respectively (see the text). The inset shows the inverse ESR intensity which is proportional to the inverse spin susceptibility. The straight line corresponds to a Curie–Weiss law for $T > 100$ K. The deviations below $T < 100$ K is due to the splitting of the main resonance line.

with a typical energy splitting of 10^3 K. In this case the four 3d electrons will generate a $^5B_{1g}$ ground state for axially elongated octahedra, corresponding to a spin quintuplet with the usual Zeeman effect [12]. Therefore, the observation of the broad resonance becomes possible due to a pronounced Jahn–Teller effect.

3.3. Weak resonance

We now turn to the small resonance around $B_{res} \approx 0.33$ T. Neither the linewidth nor the resonance field displayed any significant directional dependence within the experimental accuracy. Their temperature dependences together with the intensity are shown in figure 6 for $\vec{B} \parallel \vec{a}$ and $\vec{h} \parallel \vec{b}$. From room temperature down to $T = 100$ K, the linewidth, intensity and resonance field remain almost constant. Below $T = 70$ K, the linewidth starts to increase to lower temperatures; this is accompanied by a small drop of the resonance field. The inverse ESR intensity is shown in the inset of figure 6. At high temperatures $T \geqslant 100$ K, well within the paramagnetic regime, the intensity follows a Curie–Weiss law with the same Curie–Weiss temperature $\Theta = -68$ K as was observed for the main resonance. At low temperatures, the inverse intensity exhibits a pure Curie behaviour ($\Theta = 0$) with a different slope.

As mentioned above, the broad resonance represents by far the major part of the total ESR intensity (corresponding to the spin susceptibility of the compound). The intensity ratio

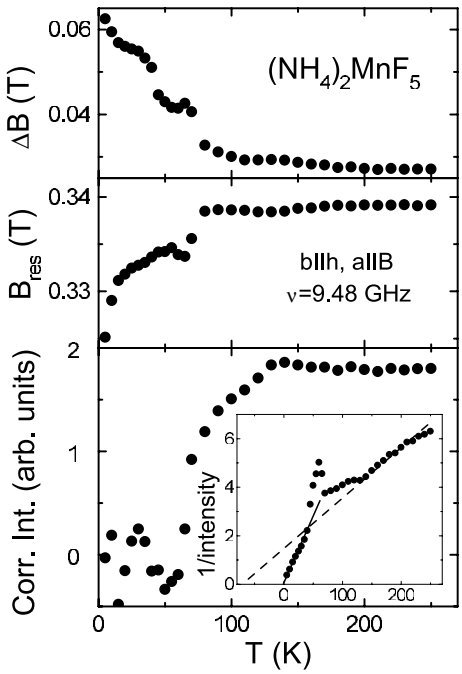

Figure 6. Temperature dependences of the linewidth (upper panel), resonance field (middle panel) and ESR intensity corrected for a low-temperature Curie term (lower frame) of the small resonance for $(NH_4)_2MnF_5$. The inset shows the inverse intensity versus temperature following a Curie–Weiss behaviour at high temperatures (dashed line) and a Curie behaviour at low temperatures (solid line).

of the small and broad resonance is approximately 10^{-3}. This demonstrates that only $\approx$0.1% of the spins contribute to the weak signal. We therefore attribute this contribution as arising from defects of the sample. For example, F^- vacancies would result in Mn^{2+} ions with a much smaller single-ion anisotropy, because with its half-filled 3d shell Mn^{2+} is a pure S-state ion. Furthermore, paramagnetic centres at the end of a chain can also give a contribution to the weak resonance. In addition, other impurities may contribute to this weak signal, though it should be noted that we have no indication of the presence of other 3d impurities on the basis of single-crystal susceptibility measurements [11]. The Curie–Weiss law ($\Theta = -68$ K) observed at high temperatures strongly supports the first possibility, of Mn^{2+} ions representing the main contribution to the weak signal. These spins take part in the dynamics of the chains as they 'feel' the full exchange interaction. At lower temperatures, the pure Curie law reveals additional defects which are only weakly coupled to the magnetic chains. Indeed, the temperature-dependent ESR intensity corrected for the low-temperature Curie term reveals, at least qualitatively, the behaviour of a one-dimensional magnet, as shown in the lower frame of figure 6. Upon entering the one-dimensional magnetic regime, the resonance becomes extremely weak as the intensity decreases towards zero.

The identification of the main defects as Mn^{2+} ions is supported by all other observations. The resonance field of the small signal corresponds to g-values of $g \approx 2.02$, whereas generally g-values slightly below the free-electron value are observed for transition metal ions with less-than-half-filled d shells. The weak signal is observed for all orientations with a rather small, nearly unchanged linewidth, in agreement with the very weak anisotropy of an S-state ion.

4. Conclusions

We have performed ESR measurements on single-crystalline $(NH_4)_2MnF_5$. For $\vec{b} \parallel \vec{h}$ we observed two contributions to the ESR signal, a broad resonance around $B_{res} \approx 0.66$ T and a narrow resonance on top of the broad signal. Due to the large linewidth of the main resonance, several typical characteristics of EPR signals of conventional 1D Heisenberg antiferromagnets like TMMC [13, 14] or $CsMnCl_3$ [15, 16] could not be observed in the present study. This includes significant deviations from a Lorentzian line shape at high temperatures well within the purely paramagnetic state and a typical $(3\cos^2\Theta - 1)^{4/3}$ angular dependence of the linewidth, with Θ being the angle between the chains and the external field. Nevertheless, we have shown that the broad line results from Mn^{3+} ions of the magnetic chains. This resonance becomes observable due to the Jahn–Teller effect, like in e.g. $LaMnO_3$ [17]. Hence, $(NH_4)_2MnF_5$ is a rare example of a compound with (high-spin) Mn^{3+} ions in an octahedral environment for which an ESR signal has been observed. The ESR line of $(NH_4)_2MnF_5$ is dominated by non-diagonal terms of the dynamic susceptibility due to the low symmetry of the interactions in one-dimensional magnetic chains. The weak resonance was mainly ascribed to Mn^{2+} ions resulting from F^- vacancies. As a result of the present study, $(NH_4)_2MnF_5$ is characterized as a one-dimensional magnet with strong on-site anisotropy like $CsNiF_3$, which shows very similar ESR properties.

Acknowledgments

This work was supported under contract No 13N6917 (EKM) and by the Deutsche Forschungsgemeinschaft (DFG) via Sonderforschungsbereich SFB 484 (Augsburg). The help and assistance of Dr S de Brion during the course of the measurements at the High-Field Laboratory, Grenoble, is gratefully acknowledged.

References

[1] For a review of experimental and theoretical work on 1D magnetism, see for example:
Mikeska H J and Steiner M 1991 *Adv. Phys.* **40** 161
[2] Massa W, Pebler J, Hahn F and Babel D 1987 *Organic and Inorganic Low-Dimensional Crystalline Materials (NATO ASI Series)* (New York: Plenum)
[3] Pebler J, Massa W, Lass H and Ziegler B 1987 *J. Solid State Chem.* **71** 87
[4] Pebler J 1989 *Inorg. Chem.* **28** 1038
[5] Frommen C and Pebler J 1995 *Hyperfine Interact.* **96** 51
[6] Frommen C, Schröder L, Bentrup U, Massa W and Pebler J 1995 *Z. Naturf.* B **50** 1227
[7] Frommen C, Mangold M and Pebler J 1996 *Z. Naturf.* A **51** 939
[8] van de Kamp R, Krimmel A, Mangold M and Pebler J 2000 *Phys. Rev.* B **61** 15 221
Steiner M, Winkelmann M, Baehr M, Hohlwein D, Krimmel A, Frommen D, Mangold M, Pebler J, Cohen J and Felner I 1998 *Physica* B **241–3** 555
[9] Benner H, Brodehl M, Seitz H and Wiese J 1983 *J. Phys. C: Solid State Phys.* **16** 6011
[10] Kubo R and Tomita K 1954 *J. Phys. Soc. Japan* **9** 888
[11] Pebler J, Frommen C, Mangold M and Treutmann W 1999 *Z. Naturf.* A **54** 317
[12] Abragham A and Bleaney B 1970 *EPR of Transition Metal Ions* (Oxford: Clarendon)
[13] Dietz R E, Merritt F R, Dingle R, Hone D, Silbernagel B G and Richards P M 1971 *Phys. Rev. Lett.* **26** 1186
[14] Tuchendler J, Magarino J and Renard J P 1979 *Phys. Rev.* B **20** 2637
[15] Tazuke Y and Nagata K 1975 *J. Phys. Soc. Japan* **38** 1003
[16] Nagata K and Hirosawa T 1976 *J. Phys. Soc. Japan* **40** 1584
[17] Ivanshin V A, Deisenhofer J, Krug von Nidda H-A, Loidl A, Mukhin A A, Balbashov A M and Eremin M V 2000 *Phys. Rev.* B **61** 6213